Available online at www.sciencedirect.com
ScienceDirect
C. R. Geoscience 341 (2009) 1003–1015
Comptes Rendus Geoscience

Tectonics

The Cuaró Mesozoic doleritic dyke swarm, southern Paraná basin, Uruguay: Examples of superimposed magnetic fabrics?

Henri Masquelin [a], Tahar Aïfa [b,*], Rossana Muzio [a], Erwan Hallot [b], Gerardo Veroslavsky [a], Laure Bonnevalle [b]

[a] *Depto. Evol. Cuencas, Facultad de Ciencias, Iguá 4225, CP 11400, Montevideo, Uruguay*
[b] *Géosciences Rennes, UMR 6118, CNRS, université de Rennes 1, bâtiment 15, campus de Beaulieu, 35042 Rennes cedex, France*

Received 10 September 2008; accepted after revision 6 July 2009
Available online 13 October 2009

Presented by Jacques Angelier

Abstract

The Cuaró intrusion swarm includes dykes and sills and represents the southern part of the plumbing system of the Paraná Large Igneous Province. Structural analysis reveals that it is emplaced in an overall north–south spreading direction and that extensional tectonics went on during a significant period of hydrothermal activity. Preliminary results of the Anisotropy of Magnetic Susceptibility (AMS) study show several magnetic fabrics, mostly carried by magnetite and maghemite, with typical oblate shapes in the sills and oblate to predominantly prolate shapes in the dykes. Most of the intrusions show superimposed magnetic fabrics in the same sampling zones. Some fabrics support interpretations in terms of magma flow, but objectively, different origins for other fabrics, especially for the superimposed ones, cannot be discarded at this stage. Some magnetic fabrics are consistent with those expected in the tectonic deformation field recorded up to the late hydrothermal event. Thus, we suspect that sub-solidus recrystallisations under tectonic stress and/or under some hydrothermal fluid flow may have induced some of the fabrics in the Cuaró intrusions. ***To cite this article: H. Masquelin et al., C. R. Geoscience 341 (2009).***
© 2009 Académie des sciences. Published by Elsevier Masson SAS. All rights reserved.

Résumé

L'essaim filonien doléritique mésozoïque du Cuaró, bassin sud du Paraná, Uruguay : exemples de fabriques magnétiques superposées ? L'essaim des intrusions du Cuaró comprend des filons et des sills. Il représente la partie méridionale du système de conduits d'alimentation de la Grande Province Magmatique du Paraná. L'analyse structurale révèle une direction moyenne d'étirement nord–sud pendant la mise en place des intrusions et la tectonique extensive s'est prolongée au cours d'une période d'activité hydrothermale significative. Les résultats préliminaires de l'étude d'Anisotropie de Susceptibilité Magnétique (ASM) montrent de nombreuses fabriques magnétiques, principalement portées par la magnétite et la maghémite, avec des formes d'ellipsoïde aplaties dans les sills et aplaties à principalement allongées dans les filons. La plupart des intrusions montrent des fabriques superposées dans les mêmes zones d'échantillonnage. Certaines sont compatibles avec une interprétation en termes d'écoulement de magma mais, objectivement, d'autres origines sont envisageables pour les autres fabriques, en particulier, celles qui sont superposées. D'autres fabriques sont cohérentes avec celles attendues dans le champ de déformation enregistré jusqu'à l'événement hydrothermal tardif. Nous suspectons donc que des recristallisations sub-solidus sous contrainte tectonique et/ou sous

* Corresponding author.
E-mail address: tahar.aifa@univ-rennes1.fr (T. Aïfa).

1631-0713/$ – see front matter © 2009 Académie des sciences. Published by Elsevier Masson SAS. All rights reserved.
doi:10.1016/j.crte.2009.07.004

un écoulement de fluide hydrothermal puissent avoir induit certaines fabriques des intrusions du Cuaró. ***Pour citer cet article : H. Masquelin et al., C. R. Geoscience 341 (2009).***

© 2009 Académie des sciences. Publié par Elsevier Masson SAS. Tous droits réservés.

Keywords: Dyke; Sill; Fabric; Mesozoic; Tectonics; Hydrothermalism; AMS; Uruguay

Mots clés : Filon ; Sill ; Fabrique ; Mésozoïque ; Tectonique ; Hydrothermalisme ; ASM ; Uruguay

1. Introduction

Mesozoic doleritic dykes and sills in the extreme South of the Paraná Large Igneous Province (PLIP) [34], northern Uruguay (Fig. 1), are emplaced in a geodynamical context which is still unclear. They may represent magmas linked to the South Atlantic Ocean rifting [22] and/or they can be linked to the Paraná plume activity [48]. Are they related to the early stages of this rifting? Did they contribute to feed lava flows in the southern part of the Paraná? or both? Answering such questions is beyond the scope of this paper but remains crucial to feed any general discussion relative to the relationships between plumes and rifting. However, those answers will depend largely on the interpretations of data, the significance of which first needs to be clarified. From results evidencing superimposed magnetic fabrics, our objective here is therefore to discuss different possible origins for these fabrics within magmatic intrusions.

The northern Uruguay intrusion swarm is composed of doleritic dykes and sills, known as the Cuaró formation. It cross-cuts geological units, from Upper Proterozoic to Cretaceous, including some basaltic lava flows of the Arapey Formation, one of the southernmost extensions of the Paraná flows [6]. The Cuaró swarm emplaced at ca. 132 Ma, as did the Arapey lavas, and may therefore correspond to a part of the PLIP plumbing system [18]. It follows the same general direction (∼ N100-120) as the eastern Paraguay and

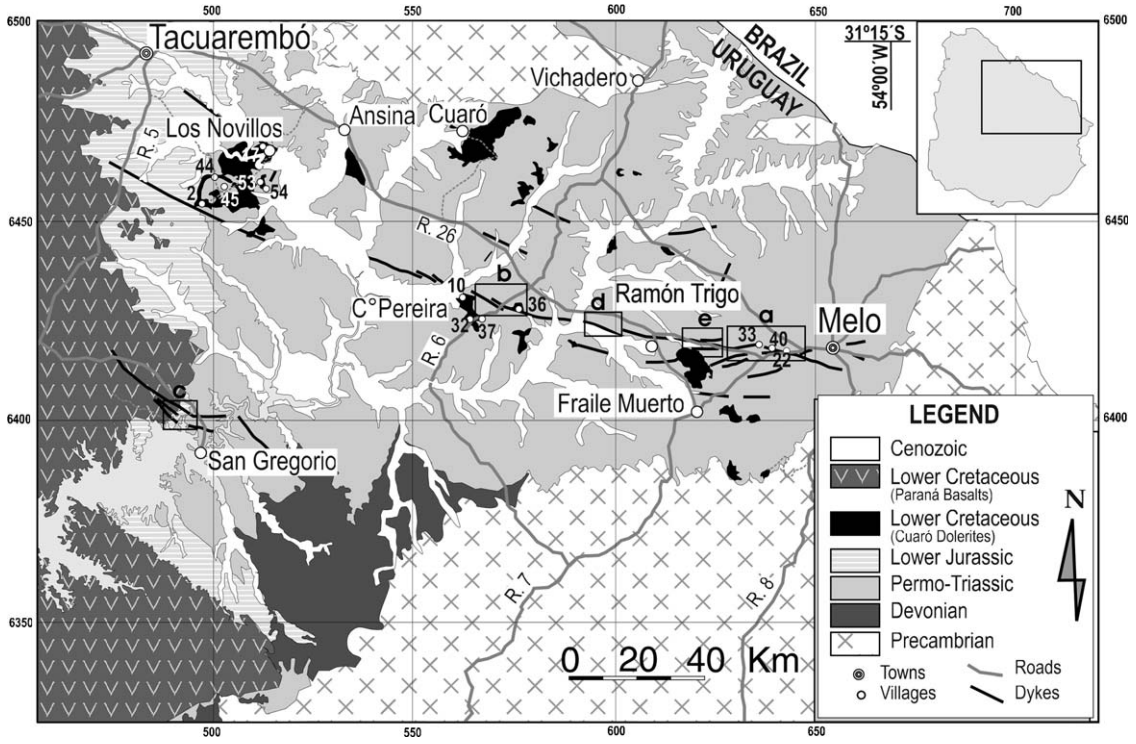

Fig. 1. Geological map of the eastern Uruguayan Paraná basin showing the sampling site locations for AMS. UTM Yacare datum projection. The rectangles represent the location of aerial photos of Fig. 2.

Fig. 1. Carte géologique de la partie orientale du bassin du Paraná, Uruguay, montrant la localisation des sites d'échantillonnage pour l'ASM. Projection UTM datum Yacaré. Les rectangles représentent les localisations des photos aériennes de la Fig. 2.

Ponta Grossa dyke swarms, belonging to the PLIP [14,37]. As in other swarms [3,10], at Ponta Grossa (Brazil), subhorizontal magma flow was evidenced [37]. However, the magma emplacement conditions (e.g. flow direction, fracturing mode) and post-emplacement events (e.g. tectonic deformation, hydrothermalism) are still not well identified in the Cuaró intrusions. Their identification is however of primary importance to make the geodynamical context clear.

The anisotropy of magnetic susceptibility (AMS) technique is an analytic method evidencing the magnetic fabric of a rock [5,30,41]. AMS was widely used on doleritic dykes to infer magmatic flow direction and tectonic deformation fields, as demonstrated by several works [1,2,5,11,12,16,23,31,33,38,40]. The method is based on the magnetic sub-fabric correlation, which is in collinear or orthogonal relationships with the petrofabric of any rock [5,31]. To infer a magmatic flow direction, the basic assumptions are:

(i) the petrofabric is representative of the flow fabric and;
(ii) the petrofabric is composed of S/C type structures related to flow [11], usually in a symmetrical arrangement relative to the dykes margins [4,21,44].

For magnetite, the AMS primarily defines the shape anisotropy of grain aggregates. For non ferromagnetic minerals, the AMS shows a crystallographic or lattice control of the vectorial magnetic properties [24]. For this reason, one can infer the orientation/distribution of a dominant mineral phase using the magnetic fabric [24].

When possible, our sampling strategy was based on coring regularly spaced oriented samples along perpendicular and/or parallel sections from one or both margins of an intrusion. Such a strategy is helpful to detect any orientation change of magnetic fabrics related to flow from the margins to the intrusion centre, especially within thick intrusions possibly resulting from multiple injections. It is also possible with such a strategy to evidence syn- to post-emplacement deformations, as it has been done in dykes emplaced in a variety of tectonic settings by combining AMS data and field observations (slickenlines, dips, orientations...).

Magnetic fabric parameters are useful in order to make out whether a fabric results from magma flow during dyking or from other events (e.g. recrystallizations during deformation and/or during fluid circulations) or origins [32,38,43]. In the best cases, knowing the relationships between AMS fabric and magma flow, the AMS data allow to deduce a tectonic deformation field during dyking [1]. Nevertheless, we can confidently associate the AMS data with a particular tectonic deformation field, if we know the absolute or relative age of the magnetic minerals carrying a given fabric. Most often, this never occurs, except when a set of samples gives superimposed magnetic fabrics carried by different mineral phases. In such a case, it becomes possible to discuss ways of discriminating between fabrics due to magma flow formed above the solidus, from fabrics due to partial or total recrystallisations in a stress field and/or due to fluid circulations linked to any hydrothermal event during or after cooling.

The purpose of this contribution is to exemplify the AMS signatures of some of the Cuaró intrusions and to discuss the origins of the fabrics in terms of primary (temperature above solidus: e.g. magma flow) or secondary post-emplacement processes (tectonic deformation and/or hydrothermal alteration) affecting dykes and sills. Geodynamics is not the aim of this work.

2. Geological setting

A synthetic overview of Mesozoic magmatism in Uruguay is given by Muzio [34]. The first studies of subvolcanic rocks in the Uruguayan Paraná basin only consider the post-Permian doleritic dykes from the area of Melo [46,47]. At first, the sills were considered as ''intrusive basalts'' [17]. Then they were assimilated to lava flows in the lateral continuity of those of the Paraná [9] before their intrusive nature was confirmed near the village of Cuaró [36], and later, in other areas within the basin (i.e. Los Novillos, Cerro Pereira and Ramón Trigo; Fig. 1) [7,8]. All the magmatic intrusions (dykes and sills) were formally defined as the Cuaró Formation and considered Triassic in age by Preciozzi et al. [36].

The sills are almost horizontal with tabular shapes but locally top contacts present significant dips. Their thickness is variable but can be estimated up to some tens of meters. The most extended Los Novillos sill has an exposure of ca. 1200 km^2, followed by the Cuaró sill, with an exposure of ca. 1000 km^2. Low-grade contact metamorphism has been recognized in the Permian sedimentary host rocks, as well as roof – pendants included in the doleritic mass.

The dykes are not homogeneously distributed. They can be grouped into two main swarms: the central (Melo – Caraguatá) and southwestern swarms (San Gregorio). They are mostly subvertical and show widths ranging between 1 and 20 m. Close to sills, they can exceed 50 m. They cross-cut Permian sediments as well as Cretaceous basaltic lava flows. On aerial photographs, dykes trend from N80° to N150°, but generally close to

N120°; there are also N20° trending dykes. A contact metamorphism is described within the walls of some dykes, where silicified sandstones and conglomerates are present. Chilled margins and hydrothermal veining are also present. Most of the dolerites in both dykes and sills present similar microgranular to granular porphyritic textures and the following mineral assemblage: Plagioclase (An_{35-50}) + Clinopyroxene (Augite) + Olivine ± opaque minerals, confirming historical observations [8,46].

We did not observe direct evidence of multiple injections within the intrusions (no internal chilled margins and/or significant grain-size variations across the width of the intrusions) but a single site 40A gave evidence for composite flow involving coeval magmas with complex mingling structures (rounded enclaves; ''cauliflower-shaped contacts''). At this site, the main magma is represented by the classical dolerite and the other occurs as a finer grained dolerite. In addition, none of the sills provides evidence for phenocryst accumulation nor cumulate textures.

Despite their regional structural trends and their spatial and temporal relationship with tholeiitic basalts of the PLIP, few authors accepted to consider them as the feeders of the Paraná basalts. In contrast, they have been considered as independent ''intra-cratonic'' magmatism and feeder channels of eroded older basaltic lava flows [7]. Féraud et al. [18] were the first to relay the sills and the dykes with the PLIP.

Doleritic bodies are here considered as the magmatic feeders through which basaltic magmas gave rise to the huge amount of the PLIP lava flows. Although some intrusions are possibly older, it is commonly accepted that the bulk magmatism was emplaced in a short time span at ca. 132 Ma at the beginning of the opening of the South Atlantic Ocean [14,19,39]. Yet, there is not enough evidence that dolerites intruded in a single magmatic event. Only two $^{40}Ar/^{39}Ar$ ages are available at 131.6 ± 1.3 Ma on a dyke and 132.1 ± 1.06 Ma on a sill [45]. Most available K/Ar ages are younger and range from 121 ± 6 to 131.8 ± 6.4 Ma [34]. If we interpret them as cooling ages, they become compatible with a main intrusive event at ca.132 Ma followed by a significant period of hydrothermal activity.

3. Structural data

Our fieldwork was focused on the western Melo region, where the number of dykes is larger and better exposed than elsewhere. The most conspicuous sills were also studied (i.e. Los Novillos, Cerro Pereira and Cuaró). Geological maps at 1:50,000 are still not available in the study area. The tectonic evolution of the Paraná basin, Uruguay is not well constrained yet.

The dyke swarm structural analysis was made using photo-interpretation analysis. Some dykes are segmented (Fig. 2a). Branching-dykes are common (Fig. 2a–e) as well as angular jogs in relay zones (Fig. 2a,d). Local ''en-echelon'' dyke distribution was recognized, indicating that sinistral (Fig. 2b) and dextral (Fig. 2d) strike-slip movements, depending on the dyke swarm orientation, occurred during dyking. Others show kinks and local bending (Fig. 2c,e). The dykes are closely linked to sills (Fig. 2b). Although we did not observe directly a dyke transforming into a sill, such feature has been previously described [8]. Most of these structures and the general trend of the dyke arrays suggest a north–south to NNE–SSW finite extension direction, synchronous with dyking.

Mesoscale structural analyses show that the dykes as well as their host rocks are affected by a brittle extensional deformation. Normal fault-planes contain slickensides showing a dip-slip sense of shear (Fig. 3a). They are concentrated in two main families (Fig. 3b). Their directions were observed to be mostly subparallel to the dyke margins. Slickenline contour plot shows mainly two maxima distributions plunging in opposite directions, to the north and to the south (Fig. 3c). The brittle fault was recorded after the cooling of the magma but fracturing was observed to be synchronous with a hydrothermal activity, which is recorded by the presence of hematite, calcite or silica veinlets within both the dykes and their host rocks. Dip-slip slickensides on hydrothermal veins show the synchronicity between hydrothermal fluid circulations and faulting. Hydrothermal activity may locally be recorded by a strong alteration within the doleritic mass, especially along some margins. Along some normal faults, the development of doleritic breccias shows that host rock sediments were fluidized during deformation and re-injected into the solidified magma.

Most slickensides show a quasi north–south finite extension direction during the hydrothermal event. The mean main trend for dykes gives almost the same finite extensional direction, suggesting that the hydrothermalism directly relates to the magmatic event. We conclude that dyking and subsequent hydrothermalism occurred in a bulk north–south finite extensional direction.

4. Anisotropy of magnetic susceptibility data

Among 55 doleritic outcrops visited, most were not suitable for magnetic studies because of alteration and bad outcrop conditions. However, 13 sampling sites

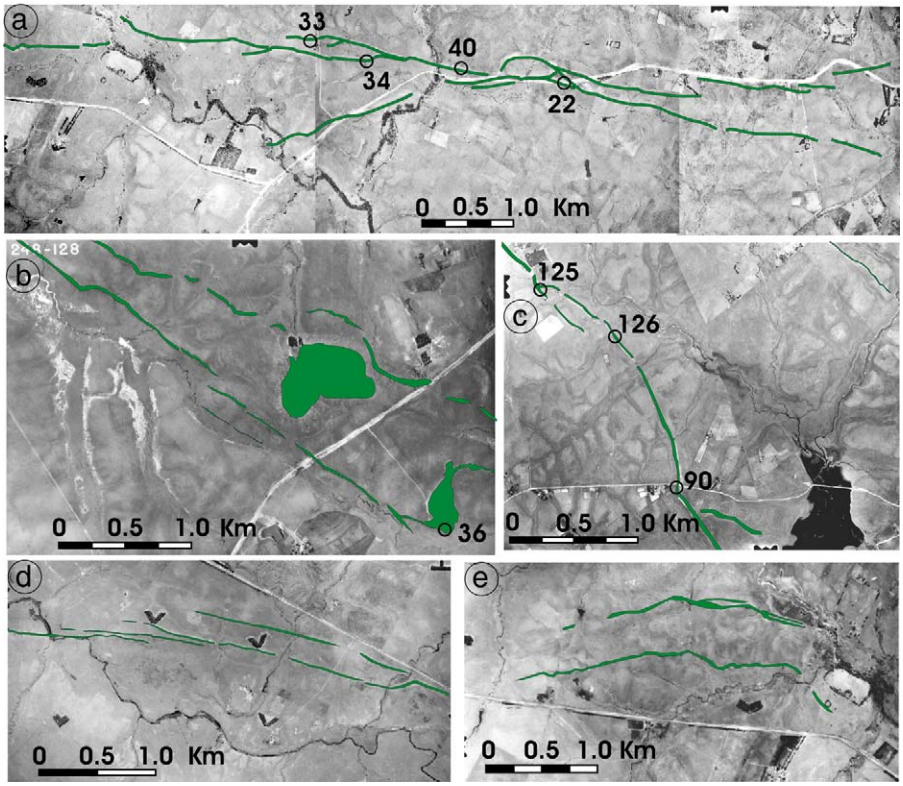

Fig. 2. Different outcropping dyke arrays of the Paraná Basin in Uruguay. (**a**) Branching dykes (western Melo). (**b**) Sinistral shearing and sill relay (Caraguatá). (**c**) Branching dykes and local bending (San Gregorio de Polanco). (**d**) ''En-echelon'' geometry giving dextral shearing (Bañado de Medina, road 26). (**e**) Two parallel kinked dykes (Bañado de Medina, road 26).

Fig. 2. Différentes géométries de filons affleurant dans le bassin du Paraná en Uruguay. (**a**) Ramification de filons (ouest de Melo). (**b**) Cisaillement sénestre avec connexion en sill (Caraguatá). (**c**) Ramification de filons et courbure locale (San Gregorio de Polanco). (**d**) Géométrie « en-échelon » montrant un cisaillement dextre (Bañado de Medina, route 26). (**e**) Deux filons parallèles avec des genoux (Bañado de Medina, route 26).

(9 sills and 4 dykes) were selected and 452 specimens were collected (Fig. 1). From these specimens, only 439 specimens were used for the statistics; some of the remaining specimens were used for thin sections and rock magnetic analyses. Sampling was made as close as possible to the margins of the intrusions but most of the cores were taken at a distance of several metres from the contacts (Table 1 gives estimates of the distances of the groups of samples from the contacts). Samples were cored parallel and/or perpendicular to the contacts.

Bulk magnetic susceptibility was measured using a KLY-3 kappabridge (AGICO, Brno) and gave values ranging between 0.38×10^{-4} and 1.142×10^{-1} SI, with a corrected degree of anisotropy P′ indicating an anisotropy between 0.1 and 12% except for two specimens which reach 25% (in Table 1, the mean sampling site values never exceed 10%; the anisotropy percentage is calculated using 100(P′-1)). In both sills and dykes, different fabrics were evidenced by selecting samples showing coherent clustering of the AMS tensor's main axes calculated from bootstrap statistics [44]. We verified afterward if the fabrics do or do not depend on the spatial distribution of the samples in each site.

The sills gave relatively fresh dolerite samples. The shape parameter (T) indicates mostly oblate ellipsoids, the bulk magnetic susceptibility ranges between 3.8×10^{-4} and 3.6×10^{-2} SI and the anisotropy is low, between 1.1 and 2.2% (Table 1). AMS tensor's minimum axes (K_3) are mainly subvertical, perpendicular to the intrusive contacts. Except for sites 53 and 54 (Fig. 4a) where a single fabric is recorded, in the seven other sills, one to two additional fabric(s) can be evidenced (Table 1). For some of these additional fabrics, K_3 remains subvertical. In the concerned sites, a switch between subhorizontal K_1 and K_2, most often independent on the spatial distribution of the samples, can be observed (fabrics 2-1 compared to 2-2,17-1 to 17-2, 32-1 to 32-3, 45-1 to 45-2 in Table 1). In the other cases, K_3 is no longer subvertical (fabrics 10-2

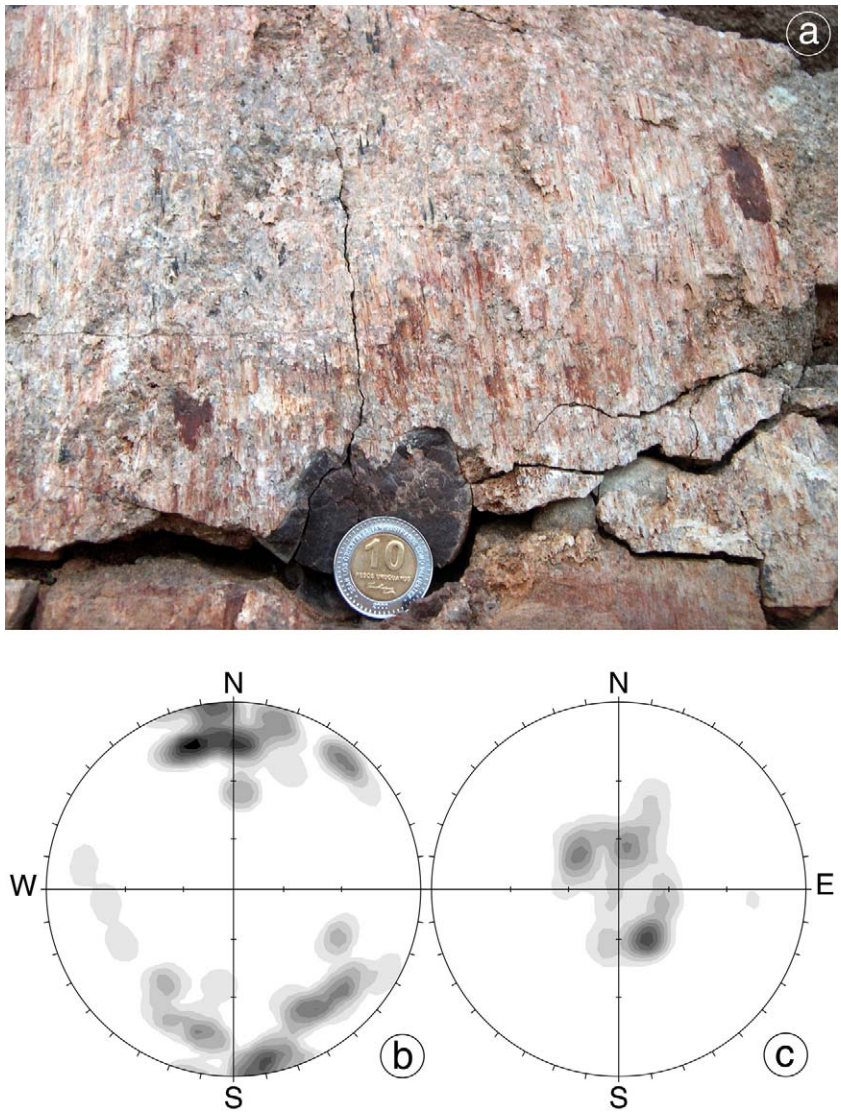

Fig. 3. Dip-slip slickensides at Melo (site 22). (**a**) Photograph of dip-slip slickenlines at the contact interface between the dyke and the wall of the host rock. (**b**) Fault plane poles ($n = 54$) and (**c**) Slickenlines ($n = 54$) using Kamb's [29] contouring method on lower hemisphere equal area projections, in agreement with the photograph.

Fig. 3. Plans de faille avec des stries pleine pente à Melo (site 22). (**a**) Photo de stries pleine pente sur un contact encaissant–filon. (**b**) Pôles de failles ($n = 54$) et (**c**) Stries ($n = 54$) en projections à aire égale de l'hémisphère inférieur, utilisant la méthode des contours de Kamb [29], en accord avec la photo.

compared to 10-1, 32-2 to 32-1, 36-2 to 36-1, 37-2 to 37-1, 45-3 to 45-1 in Table 1 and Fig. 4b,c). These additional fabrics are most often dependent on the spatial distribution of the samples relative to the contacts.

The anisotropy in dykes (up to 10%) is larger than in sills, and T exhibits both prolate and oblate signatures, often predominantly prolate. Three fabric types are evidenced in Table 1: a- K_3 almost perpendicular to the dyke walls and subhorizontal K_1 or K_2 (normal fabrics 33-1, 33-2, 40A-1 and 44; Fig. 4e,f); b- K_1 almost perpendicular to the dyke walls and subvertical or steep K_3 (inverse fabrics 22-1, 40A-3 and 40B-3); c- K_2 almost perpendicular to the dyke walls (intermediate fabrics 22-2, 40A-2, 40A-4, 40B-1 and 40B-2). In site 22, fabrics 22-1 and 22-2 do not depend on the spatial distribution of the samples from the dyke margins. This is also the case in sites 40A and 40B. In addition, in 40A where two different dolerites mingle, the fabrics are observed to be independent from the rock type. Fabrics

Table 1
AMS parameters of the Cuaró intrusions. Sampling sites located on Fig. 1, are identified by numbers with superscripts refering to GPS (W, S) coordinates, given at the bottom of the Table; A, B, C are used to distinguish sample groups within a sampling site; obs.: indicates the approximate location of groups of samples, relative to the bottom (b) or top (T) contacts of the sills, relative to the North (N) contacts for the dykes (in brackets are the distances from the contacts b, T, N or between sample groups; u: undefined distance; c: chilled margin); -1,-2,-3 or -4 distinguishes between different fabrics (Fi) within a sampling site; *n*: number of samples; K_m: bulk magnetic susceptibility; DK_i/IK_i: declination/inclination of the maximum ($i = 1$), intermediate ($i = 2$) and minimum ($i = 3$) susceptibility principal axes and their oval of 95% confidence about the mean (α_{95}); P', T: mean corrected degree of anisotropy and shape parameter [26,27].

Tableau 1
Paramètres d'ASM des intrusions du Cuaró. Les sites d'échantillonnage, localisés en Fig. 1, sont identifiés par des numéros avec des exposants indiquant leurs coordonnées GPS (W, S), données en bas de tableau ; A, B, C sont utilisés pour distinguer les différents groupes d'échantillons dans un même site ; obs. : localisation spatiale des groupes d'échantillons par rapport au contact bas (b) ou haut (T) des sills, par rapport au contact nord (N) des filons (entre parenthèses : distances des contacts b, T, N ou entre groupes d'échantillons ; u : contact indéfini, c : marge figée) ; -1,-2,-3 ou -4 : différentes fabriques (Fi) d'un site ; *n* : nombre d'échantillons ; K_m : susceptibilité magnétique moyenne ; DK_i/IK_i : déclinaison/inclinaison des axes de susceptibilité maximum ($i = 1$), intermédiaire ($i = 2$) et minimum ($i = 3$) et leur ellipse de confiance à la probabilité de 95 % (α_{95}) ; P', T : degré d'anisotropie corrigé et paramètre de forme moyens [26,27].

Site	Obs.	Fi	*n*	$K_m \pm SD$ (10^{-3} SI)	DK_1/IK_1	α_{95}	DK_2/IK_2	α_{95}	DK_3/IK_3	α_{95}	P'	T
9 Sills												
2[1]	T (≈10 m)	2-1	24	18.8±1.8	348.6/0.7	17.9/5.1	258.6/2.1	17.9/6.3	96.8/87.7	6.7/4.6	1.013	0.560
	T (≈10 m)	2-2	8	18.6±1.0	249.4/2.3	32.2/5.3	159.3/2.6	31.7/9.6	21.2/86.6	9.9/8.1	1.010	0.726
10A[2]	b (< 0.2 m),c	10-1	5	19.3±2.7	189.2/1.5	32.3/9.2	279.5/9.9	42.6/22.4	90.4/80.0	38.4/9.3	1.044	0.599
10B[2]	(≈2 m above, ≈20 m N from 10A)	10-2	10	2.0±2.7	242.8/3.5	29.0/11.7	335.9/41.5	49.5/21.7	148.8/48.3	49.5/19.6	1.004	−0.129
17[3]	T (u)	17-1	26	17.7±1.5	126.2/2.1	22.8/3.2	216.3/1.6	22.7/7.8	344.1/87.4	8.0/3.6	1.015	0.724
	T (u)	17-2	9	18.9±1.9	42.5/3.5	27.9/4.8	132.7/3.3	27.9/5.0	266.4/85.2	5.7/4.4	1.016	0.682
32[4]	T (u)	32-1	31	27.7±5.1	146.8/4.7	23.2/10.3	55.8/12.6	37.3/13.3	257.0/76.5	38.7/16.9	1.011	−0.511
	T (u)	32-2	21	22.5±2.8	238.8/83.1	18.8/6.6	335.4/0.8	44.8/6.8	65.5/6.9	45.3/15.3	1.020	−0.395
	T (u)	32-3	16	24.7±4.7	60.8/24.7	21.9/16.4	321.4/19.5	41.1/19.2	197.4/57.7	40.5/16.8	1.015	−0.430
36A[5]	T (> 5 m)	36-1	5	11.1±1.6	114.4/23.0	20.1/5.7	12.3/26.2	52.5/5.2	239.9/53.9	52.2/9.0	1.014	−0.728
36B[5]	(≈1 m above,≈12 m N from 36A)	36-2	5	11.6±1.9	199.2/67.5	18.7/7.2	0.3/21.4	18.4/2.8	92.9/6.6	8.3/1.7	1.022	0.695
37[6]	b (≈1.5 m)	37-1	17	19.3±1.5	90.9/2.5	13.9/7.8	181.1/5.9	14.9/10.9	338.4/83.6	12.8/6.9	1.012	0.057
	b (≈1 m)	37-2	5	25.8±2.5	197.7/82.8	11.8/3.5	14.6/7.2	18.7/10.4	104.6/0.4	18/3.6	1.028	0.070
45A[7]	T (3–5 m)	45-1	11	6.9±2.9	129.8/4.7	25.2/7.9	221.0/13.5	23.3/5.6	21.1/75.7	17.3/3.3	1.006	−0.139
45B[7]	T (≈2 m)	45-2	17	7.7±2.5	66.8/19.5	21.5/9.5	158.6/5.2	25.0/12.7	263.0/69.8	21.7/9.8	1.005	−0.145
45C[7]	T (≈1 m)	45-3	5	9.0±2.6	114.8/79.4	27.4/4.7	325.1/9.2	29.7/5.7	234.2/5.3	37.0/7.2	1.008	−0.451
53[8]	T (< 3 m)		11	16.0±2.4	53.8/11.3	6.3/3.4	318.8/23.2	28.0/3.4	167.8/63.9	28.0/6.2	1.004	−0.255
54[9]	T (≈10 m)		35	17.6±1.8	221.3/23.1	20.8/7.0	311.6/0.7	20.9/8.8	43.2/66.9	9.9/6.3	1.013	0.590
4 Dykes												
22[10]	N (2–6 m)	22-1	15	18.8±4.3	211.9/7.5	29.1/20.1	302.1/1.7	30.4/18.7	44.9/82.3	26.8/14.8	1.044	0.192
	N (2–6 m)	22-2	15	22.6±2.7	59.8/74.4	15.3/11.9	186.3/9.4	21.7/8.5	278.3/12.3	20.4/15.1	1.050	−0.394
33[11]	N (3-5 m)	33-1	9	16.9±1.7	257.1/12.2	6.5/2.6	23.1/69.9	10.2/2.9	163.6/15.8	10.4/6.0	1.027	−0.181
	N (3–5 m)	33-2	24	20.1±3.3	302.9/69.7	14.6/5.0	68.3/12.1	14.6/10.2	161.8/16.0	10.2/5.0	1.041	−0.184
40A[12]	N (3–10 m)	40A-1	16	46.1±31.7	64.8/58.5	22.0/11.7	284.3/25.3	21.9/15.7	185.7/17.5	15.7/12.0	1.044	−0.049
	N (3–10 m)	40A-2	14	26.9±10.1	46.5/66.7	15.6/13.0	172.5/14.2	32.3/12.9	267.3/18.1	32.8/14.0	1.041	−0.543
	N (3–10 m)	40A-3	9	25.8±7.2	171.8/7.9	21.3/9.5	266.5/30.2	2.0/8.2	68.7/58.6	3 27.1/10.2	1.038	0.008
	N (3–10 m)	40A-4	9	37.7±26.2	248.8/38.3	53.1/30.2	156.3/3.2	54.5/33.4	62.2/51.6	42.0/21.6	1.023	0.115

Table 1 (*Continued*)

Site	Obs.	Fi	*n*	$K_m \pm SD$ (10^{-3} SI)	DK_1/IK_1	α_{95}	DK_2/IK_2	α_{95}	DK_3/IK_3	α_{95}	P'	T
40B[12]	N (≈6 m),30 m W from 40A	40B-1	5	18.3±4.16	315.6/10.1	4.0/3.0	48.4/15.4	9.6/3.0	193.7/71.4	10.1/1.7	1.056	−0.199
	N (≈6 m),30 m W from 40A	40B-2	5	17.2±2.8	136.6/63.3	5.0/2.9	11.2/16.3	26.4/2.8	274.9/20.6	26.6/3.0	1.056	−0.609
	N (≈6 m),30 m W from 40A	40B-3	14	15.2±4.3	181.4/24.1	14.7/8.3	77.5/28.2	34.5/12.8	305.4/51.4	34.1/7.9	1.079	−0.593
44[13]	N (≈50 m)		43	41.3±8.1	328.2/64.3	11.8/10.7	73.1/7.0	21.3/11.8	166.3/24.6	21.2/10.7	1.051	−0.368

[1]55°07'07", 32°17'48", [2]55°49'13", 32°02'40", [3]55°40'32", 31°57'55", [4]55°07'04", 32°18'20", [5]55°02'24", 32°16'21", [6]55°05'49", 32°18'27", [7]55°47'47", 32°00'02", [8]55°44'38", 32°00'20", [9]55°41'58", 32°00'04", [10]54°18'46", 32°22'43", [11]54°20'45", 32°22'26", [12]54°19'29", 32°22'37", [13]55°47'59", 32°22'37".

33-1 and 33-2 are partly dependent on the spatial distribution of the samples. In the site 33, coring was made in a rectangular zone 2 m wide (3 to 5 m from the northern contact, Table 1) and 6 m long parallel to the contact. Most of the samples of the eastern part of the sampling zone define the fabric 33-1 while most of the samples of the western part define the fabric 33-2 but sometimes, as in other sites, the same core exhibits different fabrics in different samples.

5. Discussion and conclusions

On the bases of available radiometric data [45], previous descriptions [8] and from our own structural (Fig. 2a) and petrological observations, we are confident that most dykes and sills relate to a single main magmatic event. The structural data (e.g. dyke arrays, dyke contact orientations, normal faults and slickensides) show a predominantly NW–SE trend for the dykes (Fig. 1) and a dominant east–west trend for the normal fault planes (Fig. 3b). Normal faults are subparallel to the dyke segments, which are not systematically parallel to the general dyke trend. These structural features and geological observations document a general north–south extension synchronous with dyking and subsequent hydrothermal activity. The presence of micro-cracks and hydrothermal minerals in the dykes indicates that magnetic fabric could secondarily have been influenced by the deformation associated with hydrothermalism. Additional late (post-cooling) faulting may also affect some intrusions.

In sills, magnetic fabrics are mostly oblate with K_3 perpendicular to the margins. This suggests that most fabrics probably relate to their primary (magmatic) petrofabric. These primary fabrics, acquired above solidus temperatures, may directly reflect magma flow directions during magma emplacement [41]. In such a case, subhorizontal K_1 or K_2 are compatible with magma flow (Fig. 4a,b). During the crystallization of the magma, they may also result from crystal settling [35] in a stagnant magma (weak P', $K_1 \sim K_2$) but we have no petrological evidence of cumulative textures, or result from vertical compaction of a magmatic mush under the weight of the sediments above the sills. In addition, such fabrics can also be secondary, that is acquired at sub-solidus temperatures: a vertical K_3 is also consistent with the vertical shortening expected in an extensional setting. In such case, sub-solidus re-equilibrations of some of the magnetic minerals should have occurred within the sills. Objectively, our results on sills are not helpful to discriminate between these different primary and secondary processes (flow,

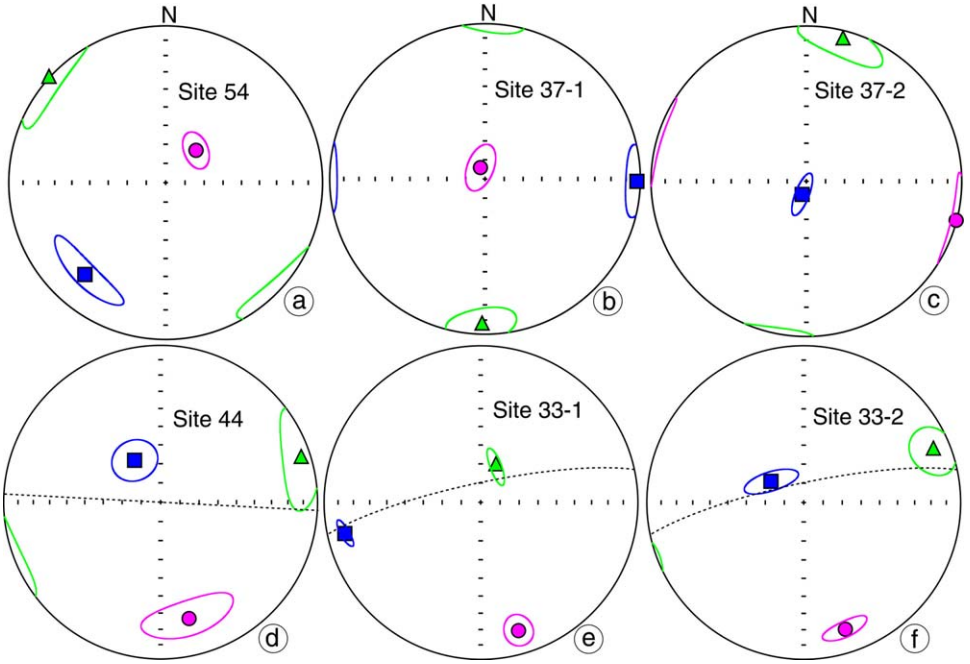

Fig. 4. Lower hemisphere equal area projections of AMS tensor principal axes [26] for sills (**a,b,c**) and dykes (**d,e,f**). Example of a sill (**a**, dip ∼10°E) and a dyke (**d**) which did not record superimposed fabrics. Example of two superimposed fabrics on a sill (**b,c**) with a vertical K_3 and a horizontal magma flow (site 37) and on a dyke (**e,f**) with a horizontal magma flow (site 33) superimposed on a vertical component. The dashed lines represent the trace of the dykes.

Fig. 4. Projections à aires égales dans l'hémisphère inférieur des axes principaux du tenseur d'ASM [26] pour des sills (**a,b,c**) et des filons (**d,e,f**). Exemple de sill (**a**, pendage ∼10°E) et de filon (**d**) qui n'ont pas enregistré de fabriques superposées. Exemple de deux fabriques superposées dans un sill (**b,c**) avec un K_3 vertical à et un flux magmatique subhorizontal (site 37) et dans un filon (**e,f**) avec un flux magmatique horizontal (site 33) superposé à une composante verticale. Les tiretés représentent la trace du filon.

compaction and sub-solidus recrystallization under stress). Nevertheless, thermomagnetic curves within sill 37 (Fig. 6a) show three different magnetic carriers: one is likely magnetite, with a Curie temperature at ∼570 °C, the others, with lower Curie temperatures at ∼520 °C and ∼200 °C, are probably maghemite and undetermined impure phases (goethite? maghemite? magnetite?), respectively. Fabric 37-1 is carried by magnetite and a small amount of maghemite (sample 37-12) while fabric 37-2 (sample 37-4) is carried by magnetite (in lower amount than in sample 37-12), maghemite and a small amount of impure phases (sample 37-4, Fig. 6a). Despite uncertainties on the nature of some of the magnetic phases, the magnetic mineral assemblages are clearly different from one fabric to the other. In the same rocks, these different assemblages are unlikely to have been produced in the same temperature range during cooling. Fabric 37-1, consistent with flow, is likely primary. This leads us to propose a secondary origin for fabric 37-2 (Fig. 4c) but it could also result from late stage crystallization of the magma [43]. Vertical K_1 in fabric 37-2 is inconsistent with the vertical shortening excepted during extensional deformation which unlikely explains the fabric. For this reason, we suspect that the superimposed fabric 37-2 could result from sub-solidus fluid circulations which partly transformed high temperature magnetic phases (magnetite) into lower temperature phases (maghemite).

Magnetic fabrics in dykes are more difficult to interpret than in sills. There is still a debate on the relationships between magnetic fabrics given by AMS and petrofabrics resulting from magma flow [13,43]. Normal or inverse fabrics can result from magma flow [42]. Examples of such fabrics are observed in all the dyke sites but site 33 exhibits two different normal fabrics (Fig. 4e,f) with predominantly prolate shapes (Fig. 5). Fabric 33-1 with a subhorizontal K_1, parallel to the dyke margins, suggests horizontal or vertical magma flow (Fig. 4e). It is possible that fabric 33-2 results from the same flow as examplified in a similar context [10,11] or from theoretical considerations [15,20,25,28]. However, fabric 33-2 with a subvertical K_1, is also consistent with horizontal or vertical flow.

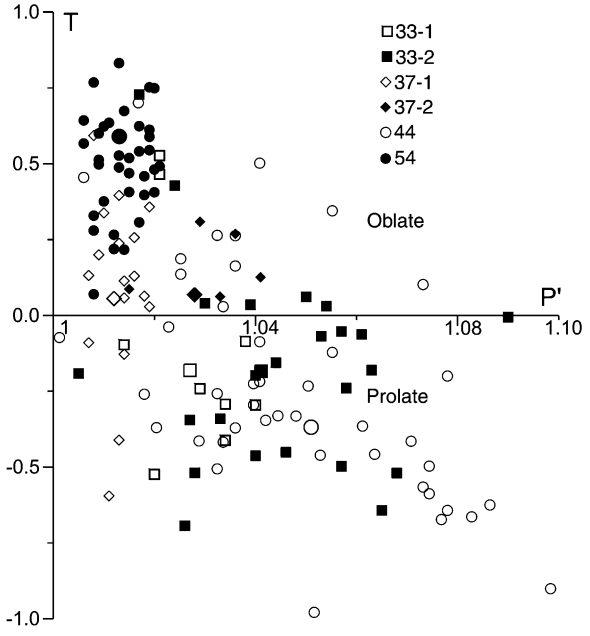

Fig. 5. Shape parameter T versus corrected degree of anisotropy P′ [26,27] for the sills (sites 37, 53) and the dykes (sites 33, 44) with their statistical mean (large symbols). 37-1 (**b**), 37-2 (**c**) and 33-1 (**e**), 33-2 (**f**) recorded superimposed fabrics while 54 (**a**) and 44 (**d**) did not (see Fig. 4 and Table 1).

Fig. 5. Paramètre de forme T en fonction du degré d'anisotropie corrigé P′ [26,27] des sills (sites 37, 53) et des filons (sites 33, 44) et leur moyenne statistique (grands symboles). 37-1 (**b**), 37-2 (**c**) et 33-1 (**e**), 33-2 (**f**) ont enregistré des fabriques superposées, alors que 54 (**a**) et 44 (**d**) n'en ont pas enregistré (cf. Fig. 4 et Tableau 1).

From thermodynamics, it is reasonable to assume that for a same magma composition, different magnetic mineral assemblages, carrying different fabrics, result from different events or temperature ranges during cooling. Thus, we used thermomagnetic curves (samples from both fabrics) to examine which of these two superimposed fabrics is more likely related to magma flow. The results from samples 33-16 (fabric 33-1) and 33-2 (fabric 33-2) are presented in Fig. 6b. They show a single magnetic carrier, likely magnetite, evidenced by a Curie temperature at ∼580 °C in fabric 33-1, and two main carriers, maghemite and magnetite in fabric 33-2 evidenced by a susceptibility drop (possibly due to a phase transformation) at ∼450 °C and a Curie temperature at ∼580 °C, respectively. Such a difference in the mineralogical assemblage suggests that only one of these two fabrics is reliable to magma flow. Even though both magnetic assemblages can be magmatic in origin, maghemite can also be of secondary origin and result from recrystallization of primary phases [43]. For this reason, we interpret fabric 33-1 as primary, resulting from magma flow (Fig. 4e). We propose that fabric 33-2 is secondary (or primary but unrelated to magma flow) and superimposes on fabric 33-1. Because maghemite can crystallize in reduced environment, it is likely that subvertical "per ascensum" fluid circulations [1] parallel to K_1 (Fig. 4f) have induced partial and/or total recrystallization. Such a hypothesis is also supported by direct field evidences of hydrothermalism. Fabric 44 compares with fabric 33-2 (Fig. 4d,f) though the outcrops are separated by more than 150 km (Fig. 1). In addition, site 44 is located at about 50 m from the northern contact of a particularly thick dyke. This distance makes it difficult to offer any interpretation of the fabric as a result of magma flow. The exceptional thickness of this dyke can be explained by the proximity (less than 200 m) of a neighbouring sill to which the dyke is probably connected.

Based on previous discussion, we attribute a primary origin to the fabrics in sills which are identified by the sub-number "-1" in Fi (Table 1), though the fabrics which are identified by the sub-number "-2" and which show a permutation between subhorizontal K_1 and K_2 may also be primary. All the other fabrics in sills are likely secondary. In dykes, primary fabrics reliable to magma flow concern fabrics 2-1, 33-1 and 40A-1. If some of the other fabrics possibly relate to magma flow, most of the ones which are superimposed likely result from late stage crystallization of the magma or secondary events (fluid circulations, tectonic deformation). Silva et al. [43] describe exsolution processes enhanced by slow cooling rates. These processes occur in magnetic minerals above and below solidus temperatures of doleritic magmas and affect the magnetic fabrics. They may also be active in our samples, especially because we have sampled thick intrusions and, most often situated several metres from the contacts.

Superimposed fabrics in sills show, from one fabric to another, permutations K_1-K_2 (e.g. site 2 or 17, Table 1) and K_1-K_3 (e.g. site 37, Fig. 4b,c). In dykes, the three permutations K_1-K_2 (e.g. site 33, Fig. 4e,f), K_1-K_3 (e.g. site 40A, fabrics 40A-1/40A-3) and K_2-K_3 (e.g. site 40A, fabrics 40A-1/40A-2) occur. If some of these permutations are explainable when the intensities of the concerned axes of the ellipsoid are approximately equal (and/or when P' is weak), they become more difficult to understand when the intensities are different in ellipsoids significantly anisotropic. In the latter case, we suspect that secondary processes (recrystallization associated or not with fluid circulations or tectonic deformation) can have been significant.

Among secondary processes involving fluids, it is difficult to discriminate between fluids associated to

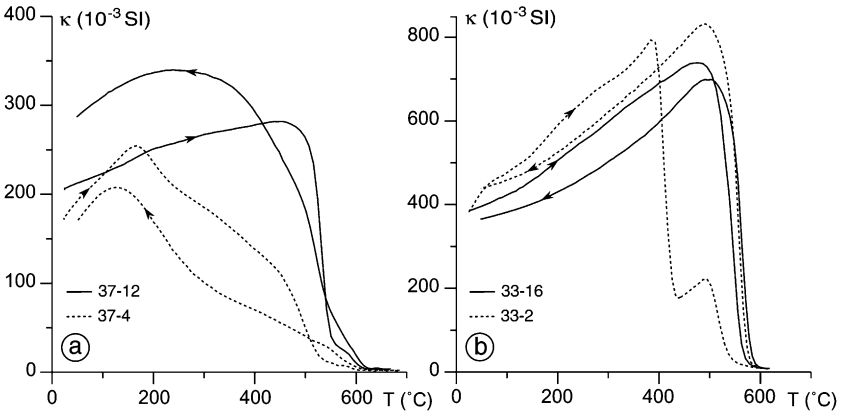

Fig. 6. Thermomagnetic curves showing two kinds of behaviours for: (**a**) sill 37: 1- sample 37-12 (fabric 37-1) shows a single Curie temperature at ∼570 °C, with an increase of magnetic susceptibility during cooling suggesting a possible transformation of the magnetic mineralogy; 2- sample 37-4 (fabric 37-2) shows two Curie temperatures, one at ∼200 °C, probably related to impure phases and the second at ∼520 °C likely of maghemite type. Arrows indicate the chronology of the experiment; (**b**) dyke 33: 1- sample 33-16 (fabric 33-1) shows a Curie temperature at ∼580 °C, probably of magnetite type; 2- sample 33-2 (fabric 33-2) shows two Curie temperatures at ∼450 °C and ∼580 °C, probably of maghemite and magnetite type, respectively.

Fig. 6. Courbes thermomagnétiques montrant deux types de comportement pour : (**a**) le sill 37 : 1- l'échantillon 37-12 (fabrique 37-1) montre une température de Curie de ∼570 °C, avec augmentation de la susceptibilité magnétique au cours du refroidissement, traduisant une possible transformation de la minéralogie magnétique ; 2- l'échantillon 37-4 (fabrique 37-2) montre deux températures de Curie, une à ∼200 °C, correspondant probablement à des phases impures et la seconde à ∼520 °C vraisemblablement de la maghémite. Les flèches indiquent la chronologie de l'expérience ; (**b**) le filon 33 : 1- l'échantillon 33-16 (fabrique 33-1) montre une température de Curie à ∼580 °C, probablement de type magnétite ; 2- l'échantillon 33-2 (fabrique 33-2) montre deux températures de Curie à ∼450 °C et ∼580 °C, probablement de type maghémite et magnétite respectivement.

magmatic events or later circulations. For example, maghemite has been related to meteoric fluid circulations associated with climatic changes [32]. However, maghemite has also been associated to changes in local stress fields [1]. Superimposed fabrics are common in many dyke swarms where interpretation of fabrics is still a matter of debate [1,13,38,43]. Further systematic sampling and analyses should help to interpret these fabrics especially in the Cuaró intrusions where they seem common. Detailed characterizations of the magnetic mineralogy, analysis of the relationships between petrological and magnetic fabrics, anisotropy of anhysteretic remanent magnetization and hysteresis loops taking into account the effects of the grain-size, are required to further interpret the origins of the superimposed fabrics that we have evidenced here in the Cuaró intrusions.

Acknowledgments

We are grateful to the ECOS-Sud project U05-U01 between France and Uruguay for the scientific exchange program and the grants for the field trips. We thank Mrs. Graciela Vigo from the French Embassy at Montevideo who helped us, particularly for the financial support of one of us (H.M.) during his stay in France. Bernard Henry helped us to obtain the thermomagnetic curves. We are greatly indebted to Bernard Henry and Jean-Paul Callot for their constructive remarks which helped us to improve the manuscript.

References

[1] T. Aïfa, J.-P. Lefort, Fossilisation des contraintes régionales miocènes sous climat aride en bordure d'un filon doléritique carbonifère en Bretagne. Apport de l'anisotropie de la susceptibilité magnétique et du paléomagnétisme, C.R. Acad. Sci. Paris Ser. IIa 330 (2000) 15–22.

[2] T. Aïfa, J.-P. Lefort, P. Gennoc, Anisotropy of magnetic susceptibility investigations of the St Malo dyke swarm (Brittany, France): Emplacement mechanism of doleritic intrusions, Geophys. J. Int. 139 (1999) 573–582.

[3] C.J. Archanjo, M.G.S. Araujo, P. Launeau, Fabric of the Rio Ceará-Mirim mafic dyke swarm (northeastern Brazil) determined by anisotropy of magnetic susceptibility and image analysis, J. Geophys. Res. 107 (2002) 1–13.

[4] J.-P. Blanchard, P. Boyer, C. Gagny, Un nouveau critère de mise en place dans une caisse filonienne : le 'pincement' des minéraux aux épontes, Tectonophysics 53 (1979) 1–25.

[5] G.J. Borradaile, B. Henry, Tectonic applications of magnetic susceptibility and its anisotropy, Earth Sci. Rev. 42 (1997) 49–93.

[6] J. Bossi, Geología del Uruguay, UdelaR- Depto. Publicaciones, Montevideo, 1966, 469 p.

[7] J. Bossi, R. Navarro, Geología del Uruguay, UdelaR, Depto. Publicaciones, Montevideo, 2 t, 1991, 968 p.

[8] J. Bossi, A. Schipilov, Rocas ígneas básicas del Uruguay, 1, Facultad de Agronomía, Universidad de la Republica, Montevideo, 1998, 245 p.

[9] J. Bossi, L.A. Ferrando, A.N. Fernández, G. Elizalde, H. Morales, J.J. Ledesma, E. Carballo, Medina, I. Ford, J.R. Montaña, Carta Geológica del Uruguay, escala 1:1.000.000, Dir. Nac. Suelos y Fertiliz., MAP, 1 mapa 1975, 32 p.
[10] J.-P. Callot, L. Geoffroy, Magma flow in the East Greenland dyke swarm inferred from study of anisotropy of magnetic susceptibility: magmatic growth of a volcanic margin, Geophys. J. Int. 159 (2004) 816–830.
[11] J.-P. Callot, X. Guichet, Rock texture and magnetic lineation in dykes: A simple analytical model, Tectonophysics 366 (2003) 207–222.
[12] J.-P. Callot, L. Geoffroy, C. Aubourg, J.P. Pozzi, D. Mege, Magma flow direction of shallow dykes from the East Greenland margin inferred from magnetic fabric studies, Tectonophysics 335 (2001) 313–329.
[13] E. Cañón-Tapia, E. Herrero-Bervera, Sampling strategies and the anisotropy of magnetic susceptibility of dykes, Tectonophysics 466 (2009) 3–17.
[14] K. Deckart, G. Féraud, L.S. Marques, H. Bertrand, New time constraints on dyke swarms related to the Paraná-Etendeka magmatic province and subsequent South Atlantic opening, southeastern Brazil, J. Volc. Geoth. Res. 80 (1998) 67–83.
[15] M. Dragoni, R. Lanza, A. Tallarico, Magnetic anisotropy produced by magma flow: theoretical and experimental data from Ferrar dolerite sills (Antarctica), Geophys. J. Int. 128 (1997) 230–240.
[16] B.B. Ellwood, Flow and emplacement direction determined for selected basaltic bodies using magnetic susceptibility anisotropy measurements, Earth Planet. Sci. Lett. 41 (1978) 254–264.
[17] J.D. Falconer, The Gondwana System of North Eastern Uruguay, Inst. Urug. Perf., Bull. 23 (1937) 1–113, 1 map.
[18] G. Féraud, H. Bertrand, M. Martinez, C. Ures, A. Schipilov, J. Bossi, ^{40}Ar-^{39}Ar age and geochemistry of the Southern Extension of Paraná Traps in Uruguay, in : III South Amer. Symp. Isotope Geol., Córdoba (Arg.), 1999, pp. 57–59.
[19] F. Garland, S. Turner, C. Hawkesworth, Shifts in the source of Paraná basalts through time, Lithos 37 (1996) 223–243.
[20] N.C. Gay, The motion of rigid particles embedded in a viscous fluid during pure shear deformation of the fluid, Tectonophysics 5 (1968) 81–88.
[21] L. Geoffroy, J.-P. Callot, C. Aubourg, M. Moreira, Magnetic and plagioclase linear fabric discrepancy in dykes: a new way to define the flow vector using magnetic foliation, Terra Nova 14 (2002) 183–190.
[22] C.J. Hawkesworth, K. Gallagher, S. Kelley, M. Mantovani, D.W. Peate, M. Regelous, N.W. Regelous, N.W. Rogers, Paraná magmatism and the opening of the South Atlantic, in : B.C. Storey, T. Alabaster, R.J. Pankhurst (Eds.),Magmatism and the Causes of Continental Break-up, Geol. Soc. Lond. 68 (Spec. Pub.) (1992) 221–240.
[23] F. Hrouda, Magnetic anisotropy and its application in geology and geophysics, Geophys. Surv. 8 (1982) 37–82.
[24] M. Jackson, L. Tauxe, Anisotropy of magnetic susceptibility and remanence: developments in the characterization of tectonic, sedimentary and igneous fabric, Rev. Geophys. 29 (1991) 371–376.
[25] G.B. Jeffery, The motion of rigid particles immersed in a viscous fluid, Proc. Roy. Soc. London, Ser. A 102 (1922) 161–179.
[26] V. Jelinek, Statistical processing of magnetic susceptibility measured in groups of specimens, Stud. Geophys. Geodetica 22 (1978) 50–62.
[27] V. Jelinek, Characterization of the magnetic fabric of rocks, Tectonophysics 79 (1981) 63–67.
[28] J. Jezek, K. Schulmann, K. Segerth, Fabric evolution of rigid inclusions during mixed coaxial and simple shear flows, Tectonophysics 257 (1996) 203–221.
[29] W.B. Kamb, Ice petrofabric observations from Blue Glacier, Washington, in relation to theory and experiments, J. Geophys. Res. 64 (1959) 1891–1909.
[30] M.A. Khan, The anisotropy of magnetic susceptibility of some igneous and metamorphic rocks, J. Geophys. Res. 67 (1962) 2867–2875.
[31] M.D. Knight, G.P.L. Walker, Magma flow directions in dikes of the Koolau Complex, Oahu, determined from magnetic fabric studies, J. Geophys. Res. 93 (1988) 4301–4319.
[32] D. Krása, E. Herrero-Bervera, Alteration induced changes of magnetic fabric as exemplified by dykes of the Koolau volcanic range, Earth Planet. Sci. Lett. 240 (2005) 445–453.
[33] J.-P. Lefort, T. Aïfa, F. Hervé, Structural and AMS study of a Miocene dyke swarm located above the Patagonian subduction, in : Hanski, Mertanen, Rämö, Vuollo (Eds.), Dyke Swarms-Time Markers of Crustal Evolution, Taylor, Francis Group, London, 2006, pp. 225–241.
[34] R. Muzio, El Magmatismo Mesozoico en Uruguay y sus recursos minerals, in: G. Veroslavsky, M. Ubilla, S. Martínez (Eds.), Cuencas sedimentarias de Uruguay: Geología, Paleontología y recursos naturales, DIRAC – UdelaR, 2003, pp. 75–100.
[35] A. Nicolas, Kinematics in magmatic rocks with special reference to gabbros, J. Petrol. 33 (1992) 891–915.
[36] F. Preciozzi, J. Spoturno, W. Heinzen, P. Rossi, Memoria Explicativa de la Carta Geológica del Uruguay a la escala 1/500.000, DINAMIGE, 1 map. Montevideo (1985).(90 p.).
[37] M.I.B. Raposo, M. Ernesto, Anisotropy of magnetic susceptibility in the Ponta Grossa dyke swarm (Brazil) and its relationship with magma flow direction, Phys. Earth. Planet. Int. 87 (1995) 183–196.
[38] M.I.B. Raposo, A.O. Chaves, P. Lojkasek-Lima, M.S. D'Agrella-Filho, W. Teixeira, Magnetic fabrics and rock magnetism of Proterozoic dike swarm from the southern São Francisco Craton, Minas Gerais State, Brazil, Tectonophysics 378 (2004) 43–63.
[39] P.R. Renne, M. Ernesto, I.G. Pacca, R.S. Coe, J.M. Glen, M. Prévot, M. Perrin, The age of Paraná flood volcanism, rifting of Gondwanaland, and the Jurassic-Cretaceous Boundary, Science 258 (1992) 975–979.
[40] P. Rochette, L. Jenatton, C. Dupuy, F. Boudier, I. Reuber, Emplacement modes of basaltic dykes in the Oman ophiolite: Evidence from magnetic anisotropy with reference to geochemical studies, in : T.J. Peters, et al. (Eds.), Ophiolite Genesis and the Evolution of the Oceanic Lithosphere., Kluwer Acad. Pub, Dordrecht, 1991, pp. 55–82.
[41] P. Rochette, M. Jackson, C. Aubourg, Rock magnetism and the interpretation of anisotropy of magnetic susceptibility, Rev. Geophys. 30 (1992) 209–226.
[42] P. Rochette, C. Aubourg, M. Perrin, Is this magnetic fabric normal? A review and case studies in volcanic formations, Tectonophysics 307 (1999) 219–234.
[43] P.S. Silva, B. Henry, F.O. Marques, E. Font, A. Mateus, R. Vegas, J.M. Miranda, R. Palomino, A. Palencia-Ortas, Magma flow, exsolution processes and rock metasomatism in the Great Messejana-Plasencia dyke (Iberian Peninsula), Geophys. J. Int. 175 (2008) 806–824.
[44] L. Tauxe, J.S. Gee, H. Staudigel, Flow directions in dikes from anisotropy of magnetic susceptibility data: The bootstrap way, J. Geophys. Res. 103 (17) (1998) 775–790.

[45] U. Ures, J. Bossi, G. Féraud, H. Bertrand, New Age and Geochemical Constraints on the Paraná Flood Volcanism: Additional Data on Uruguay Extrusive and Intrusive Formations, AGU Fall meeting, VI E-11, 1997.

[46] K. Walther, Contribución al conocimiento de las rocas basálticas de la Formación de Gondwana en la Sud-América, Bol. Inst. Geol. Perf., Montevideo 9 (1927) 1–43.

[47] K. Walther, Eruptivos afro-brasileño-argentinos de edad permo – triásico-eojurásica: La supuesta uniformidad del magma ''melafídico'' y sus relaciones con la parentela alcalinítica, Bol. Instit. Geol. del Uruguay, 1 fig., 2 pl., Montevideo 24 (1938) 117–167.

[48] M. Wilson, Magmatism and continental rifting during the opening of the South Atlantic Ocean: a consequence of Lower Cretaceous super-plume activity? in : B.C. Storey, T. Alabaster, R.J. Pankhurst (Eds.), Magmatism and the Causes of Continental Break-up, Geol. Soc. London, Spec. Pub. 68 (1992) 241–255.